Article

Hyperspectral imaging to characterize table grapes

Mario Gabrielli [1,2], Vanessa Lançon-Verdier [1], Pierre Picouet [1] and Chantal Maury [1,*]

[1] USC 1422 GRAPPE, INRA, Ecole Supérieure d'Agricultures, SFR 4207 QUASAV, 55 rue Rabelais, BP 30748, 49007 Angers Cedex 01, France: v.lancon-verdier@groupe-esa.com; p.picouet@groupe-esa.com; c.maury@groupe-esa.com

[2] Dipartimento di Scienze e Tecnologie Alimentari per una filiera agro-alimentare Sostenibile, Università Cattolica del Sacro Cuore, Via Emilia Parmense 84, 29122 Piacenza, Italy: mario.gabrielli@unicatt.it

* Author to whom correspondence should be addressed. c.maury@groupe-esa.com; Tel.: +33.241235547

Abstract: Table grape quality is of importance for consumers and thus for producers. The objective quality determination is usually destructive and very simple with the assessment of only a couple of parameters. This study proposed to evaluate the possibility of hyperspectral imaging to characterize table grapes quality through its sugar, total flavonoid and total anthocyanin contents. Different pre-treatments (WB, SNV, 1st and 2nd derivative) and different methods were tested: PLS with full spectra, then Multiple Linear Regression (MLR) were realized after selecting the optimal wavelengths thanks to the regression coefficients (⊚-coefficients) and the Variable Importance in Projection (VIP) scores from the full spectra. All models were good showing that hyperspectral imaging is a relevant method to assess sugar content and global phenolic content. The best model was dependent on the variable. The best models were from the full spectra and with the 2nd derivative pre-treatment for TSS; from VIPs optimal wavelengths using SNV pre-treatment for Total Flavonoid and total Anthocyanin content. Thus, relevant models were proposed using the full spectra, as well as specific windows and wavelengths in order to reduce the data sets and limit the data storage to enable an industrial use.

Keywords: hyperspectral imaging, phenolics, anthocyanin, table grapes, total soluble solid, PLS, MLR, model.

1. Introduction

Grapes are one of the most diffuse fruits in the world both as fresh fruit and when processed into wine, grape juice and raisins. According to the International Organization of Vine and Wine statistics, approximately 36% of world grape production is used as fresh fruit. In Europe, the production of table grapes (~1,9 million tons) remains concentrated in Mediterranean areas, and the four main producers are Italy (61%), Greece (16%), Spain (15%) and France (1,5%) [1]. The French production of table grapes is mainly placed in Vaucluse and Tarn-et-Garonne, and three cultivars represent about 80% of the production: Alphonse Lavallée, Chasselas and Muscat de Hambourg. French table grape production (~30,000 tons) accounts for approximately 40% of the national consumption, while the remainder is mainly imported from Spain and Italy.

Several studies have shown that the ripening indices such as the changes in skin color, softening, titratable acidity, soluble solids content, flavonoids and aromatic compounds are traditionally utilized to judge the right commercial harvest ripeness of table grape [2,3]. Visual attributes of table grapes, such as intensity and uniformity of color, large size of berries and brightness are the main characteristics that influence consumer choice [4,5]. Color is considered one of the most important physical properties of agro-food products and it plays a fundamental role in the assessment of external quality in food industries [6]. Furthermore, some studies have found clear evidences that a greater consumption of fresh

grapes decreases the risk of cardiovascular diseases and cancer [7,8]. This beneficial effect is mainly related to the presence of minerals, fibers, vitamins and phytochemical compounds including flavonoids and anthocyanins [9,10]. However, these quality attributes change during postharvest storage and thus influence the hedonistic and nutritional value of table grapes.

Several analytical methods have been used to evaluate the quality parameters of table grapes [11-13]. Nevertheless, conventional analytical methods are sample-destructive, time-consuming, need laborious sample preparation steps, and generate chemical waste, thereby limiting their utility in online/in-line quality monitoring [14-16]. Despite being time consuming and expensive, the destructive analytical approach provide data for a limited number of samples, and, thus, their statistical relevance could be limited [17]. Several studies in the field of post-harvest are focused on non-destructive analytical techniques which are fast, reliable, and allow to analyze a higher number of samples and repetitions of the same batch in real time.

Recently, the research has focused on the development of non-destructive techniques suitable to increase the number of samples analyzed, thus providing real-time information of quality attributes of fruits and a most robust statistical data analysis [18]. Infrared spectroscopy (FT-NIR; ATR-FTIR) has been applied for the prediction of procyanidins [19], total polyphenol content [20], malvidin-3-O-glucoside, pigmented polymers and tannins [21] in cocoa, green tea and wine, respectively. This technology has also been employed to determine, pH, total soluble solids, glycerol and gluconic acid in grape juice [22] and to measure condensed tannins and the dry matter in homogenized red grape berries [23].

Hyperspectral imaging spectroscopy (HIS) is a non-destructive spectroscopic technique that records hundreds of narrow-wavelength bands and spatial positions [24]. This technique provides a new detection method that integrates imaging and spectral techniques into a single system [25, 26], providing information on spectral response values and spatial location for each pixel in the hyperspectral image [25, 27]. A hyperspectral image is a three-dimensional (3D) hyperspectral cube that includes two-dimensional spatial information (of x rows and y columns) and one-dimensional spectral information (of λ wavelengths) [28]. The hyperspectral image cube 'hypercube' consists of a series of sub-images at small interval wavelengths ranging from 400 to 2500 nm in VIS and NIR spectral regions.

Over the last decade, HIS has been applied for fruit and vegetable quality assessment [24, 27], food safety control [29 - 31] and classification tool [32, 33]. Likewise, total acidity, pH, solid soluble content, technological maturity, total anthocyanin concentration, antioxidant activity, and total phenolic compounds in grapes were determined using VIS–NIR hyperspectral imaging of few fruits [34, 35] but a lack of study appeared for table grapes. The spectroscopic method has a great drawback compared with the HSI due to it acquires the spectral information from a small portion of the tested fruit [35, 36]. Moreover, HSI is advantageous with respect to conventional RGB techniques, which can be poor identifiers of surface features and chemical composition of the fruit sensitive to wavebands other than RGB [37]. The HIS has also advantages of receiving spatially distributed spectral responses at each pixel of a fruit image. Another advantage is once appropriate calibration models are developed, they can be re-inserted in the hypercube to create chemical mapping images.

The objective of this study was to determine if hyperspectral imaging would be able to predict the sugar content and the concentration of total flavonoids and anthocyanins of white and red table grapes. As keeping whole spectra for all samples would generate big data to manage and a higher time to analyze in a potential on-line tool, the second objective was to define if it was possible to reduce the number of wavelengths with still good

models of prediction. Thus, this study developed calibration models based on hyperspectral imaging to predict some quality attributes of table grape:

I. Developing partial least square (PLS) models to quantitatively predict total anthocyanins (TA), total flavonoids (TF) and total soluble solids content (SSC), using the visible and short-wave near-infrared region;

II. Selecting the lowest number of optimal wavelengths, based on regression coefficient (RC) and Variable Importance in Projection (VIPs) algorithms, which gave the highest correlation between the spectral data and the three selected quality parameters;

III. Developing Multiple Regression Models (MLR) using spectral responses from only the optimal wavelengths and then test and validate the prediction accuracy of the developed calibration models.

2. Materials and Methods

2.1 Chemicals

The following chemicals were used: ethanol, hydrochloric acid, (Merck-France SA); malvidin-3-glucoside (Extrasynthese, France) and (+)-catechin (Sigma–Aldrich, France). All the chemicals were at least of analytical grade. Ultrapure water was prepared from deionized water obtained a Milli-Q system (Millipore Filter Corp., USA).

2.2 Samples

Three white table grapes (Sugarone Superior Seedless, Thompson Seedless and Victoria) and four red/black table grapes (Sable Seedless, Alphonse Lavallée, Lival and Black Magic) were purchased from local fruit markets at commercial harvest ripeness. Alphonse Lavallée and Lival were chosen because they represented French cultivars produced in the south-east of France and mostly consumed throughout the country. The other 5 cultivars were chosen because they are largely diffused around the world. Approximately 5 kg of clusters randomly selected were sampled for each cultivar. Once in the laboratory, for each variety a subsample of 50 berries with short attached pedicels was collected from different bunch parts (shoulders, middle, and bottom) and stored at 4°C until the HIS acquisitions.

2.3 Hyperspectral imaging system (HIS)

The hyperspectral images of the samples were acquired by a hyperspectral system in reflectance mode.

The system is composed of the following components (Figure 1): (a) a hyperspectral imaging camera (Pika L, Resonon, USA) coupled with an objective lenses (Xenoplan 1.4/23, Schneider-Kreuznach, Germany); (c) an illumination unit which consists of four 35 W quartz tungsten halogen (QTH) MR16 35W lamps adjusted at angle of 45° to illuminate the camera's field of view; (3) a mounting tower; (d) and a transport stage (PS-12-20-1.0, Servo Systems Co., USA), with motor (DMX-J-SA-17, Arcus Technology Inc., USA). The sensor has 900 spatial channels each with 281 spectral channels covering a spectral range from 387 to 1026 nm. The maximum spectral resolution is 2.1 nm. The target was placed at a distance of 450 mm from the camera. The spectral images were collected in a dark room where only the halogen light source was used. The HIS was controlled by a PC with the software SpectrononPRO (Resonon, USA) for image acquisition.

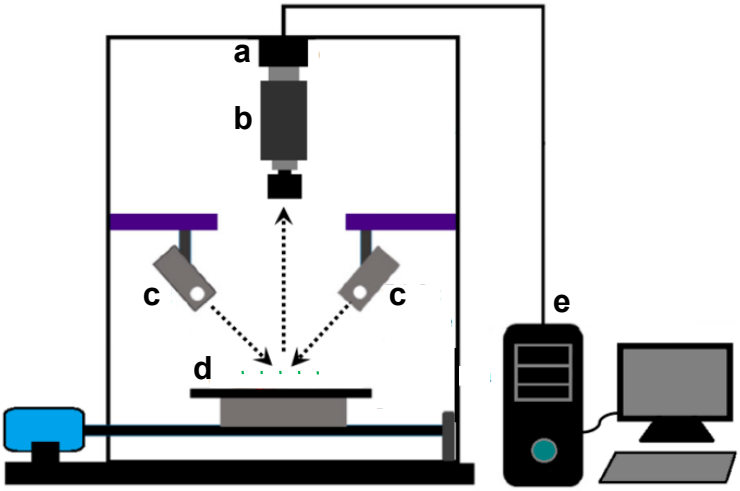

Figure 1. Hyperspectral imaging system: (a) a CCD camera, (b) a spectrograph with a standard C-mount zoom lens, (c) QTH lighting unit, (d) translation stage, and (e) a PC with image acquisition software.

2.4 Image acquisition

The samples were kept at room temperature (20°C) for 1 h prior to the imaging acquisition. The hyperspectral image of each sample (one berry) was recorded in three different berry positions corresponding to berry rotations of approximately 120° between positions. The berries reflectance measurement was made along the berry "equator" when considering the pedicel to be the "pole". This is a common practice reported by several articles [38, 39]. The hyperspectral images were recorded by the SpectrononPRO software (Resonon, USA) using an exposure time of 12 ms and a stage speed of 11 mm s^{-1} with a gain of 10. The spectral data in the wavelength range of 411–1000 nm was used in the data analysis for removing noise and reducing data redundancy out of this range. For each sample were collected three reflectance spectrums, corresponding to the berry rotations, and averaged over the spatial dimension.

2.5 Preprocessing of hyperspectral images

All the acquired images were processed and analyzed using SpectrononPro 5.1 Hyperspectral Imaging System software (Resonon, USA). The hyperspectral images were firstly corrected with a white and a dark reference. The dark reference was used to remove the effect of dark current of the CCD detectors, which are thermally sensitive.

The corrected image (R) is estimated using the following equation (1):

$$R = \frac{S - D}{W - D} * 100 \quad (1)$$

where S is the intensity of an image; W is the intensity of the white reference image (Teflon white board with 99% reflectance); and D is the intensity of the dark reference image (with 0% reflectance) recorded by turning off the lighting source with the lens of the camera completely covered. The corrected images were the basis for the subsequent image analysis to extract the spectral response of each fruit, selection of effective wavelengths and predict physicochemical parameters.

2.6 Data analysis

2.6.1 Determination of reference parameters: Soluble Solid Content (SSC) and Total Anthocyanin (TA) and Total Flavonoids (TF)

Immediately after image acquisition, each berry was subjected to the determination of soluble solid content (SSC), total flavonoids (TF) and total anthocyanins (TA). Each berry was weighed, manually peeled and the juice was collected separately. Soluble solid content was measured by a portable refractometer (Mettler Toledo Refracto 30PX). The

skins were separately weighed and, extracted four times with 7.5 mL of hydrochloride ethanol solution (ethanol / water / hydrochloric acid 70/30/1 v/v/v). The samples were shaken for 60' with a horizontal shaker VXR vibrax (IKA-Werke, Germany) at 1500 rpm, centrifuged at 5000 rpm for 5' and, the supernatant was collected a volumetric flask. The supernatants were collected together, brought to the volume of 25 mL and, stored at -80°C until analyses. The quantification of TA and TF was carried out spectrophotometrically by recording the UV-visible spectra in the range 220 to 700 nm using a Safas UV mc² spectrophotometer (Safas, Monaco) and measuring the absorption values at 280 nm and 520 nm, as previously reported [40]. The results were expressed as mg (+)-catechin equivalents/kg fresh grape and mg malvidin-3-O-glucoside equivalents/kg fresh grape for the flavonoids and anthocyanins respectively.

2.6.2 Spectral analysis for predicting quality attributes

● Collecting spectral data

Hyperspectral image extraction was performed by SpectrononPro 5.1 Hyperspectral Imaging System software (Resonon, USA). The samples were separated from the background as the regions of interest (ROIs) to reduce redundancy. To collect the spectral responses referred of each berry, the flood fill method [41] was used to isolate the ROI from the background in the score images. Then, an average reflectance spectrum was calculated by averaging the relative reflectance spectra of all the pixels selected. In total, 350 average spectra representing all the tested berries were recorded and stored in the PC for calibration model development and wavelengths selection.

● Spectra pre-treatments

To overcome or reduce unwanted spectral variation, base-line shifts, and various noise, a series of pre-treatment methods was applied on the mean spectral data to decrease the influence of high-frequency random noises, the nonuniformity in samples and the surface scattering. Before building the prediction model, different equations (2, 3 and 4) were used for spectral pre-treatments [42]:

SNV: Standard Normal Variate (SNV). The average intensity (A_{mean}) and standard deviation (A_{SD}) of the spectrum are calculated and inserted in the following equation (2):

$$B_i = \frac{A_i - A_{mean}}{A_{SD}} \quad (2)$$

1st derivative: The first derivatives A'_i was calculated using the symmetric difference quotient 1st derivative (3):

$$A'_i = \frac{A_{i+1} - A_{i-1}}{2\Delta\lambda} \quad (3)$$

2nd derivative: The second derivate A''_i was calculated using the symmetric difference quotient 2nd derivate (4):

$$A''_i = \frac{A'_{i+1} - A'_{i-1}}{2\Delta\lambda} \quad (4)$$

2.6.3 Hyperspectral imaging calibration

● Model establishment

The use of chemometrics in modeling spectral data is widely employed, being considered as a standard procedure for building predictive models in the analysis of hyperspectral images. The partial least squares (PLS) analysis between one attribute (TA; TF or SSC) and the spectral data (average spectra with 276 wavelengths in the range from 411 to 1000 nm) was conducted using XLStat software (Addinsoft 2019).

A total of 350 reflectance mean spectra were obtained from 350 berries. The calibration and validation sets were established by ordering the fruit samples according to their physicochemical references. The two highest and two lowest values were assigned to the

calibration set. Afterward, two-thirds of the samples were selected as calibration data and one-third of the samples were defined as validation data in a 2:1 leave-one-out procedure.

PLS regression used to develop calibration models for the prediction of the quality attributes, was carried out with two calibration sample sets: (i) N = 234 samples for TF & SSC; (ii) N = 133 samples for TA. The building of PLS models for the prediction of TF and SSC took into account both the white and red table grape cultivars, while for the prediction of TA was considered only the red grape cultivars since white grapes do not have anthocyanins. To reduce the probability of an over fitting of the experimental data [43], PLS models with 1-15 latent variables (LVs) were fitted, and the model with a number of PLS factors that maximized the coefficient of determination (R2cal) for the calibration and minimized the root mean square error of calibration (RMSEC) was selected. These two parameters would allow the evaluation of the models.

● Hyperspectral imaging model validation

Two validation sets (N = 116 samples for TF & SSC; N = 67 samples for TA), were used to calculate the root mean square error of prediction (RMSEP), the coefficient of determination (R^2_{val}), the Bias and the Ratio Performance Deviation (RPD) of the PLS models as follow (Picouet al., 2018):

$$\text{RMSEC} = \sqrt{\frac{1}{N-1-R}\, x \sum_{i=1}^{N}\left(y_i^{ref} - y_i\right)^2} \quad (5)$$

$$\text{RMSEP} = \sqrt{\frac{1}{N}\, x \sum_{i=1}^{N}\left(y_i^{ref} - y_i\right)^2} \quad (6)$$

$$\text{Bias} = \frac{\sum_{i=1}^{N}\left(y_i^{ref} - y_i\right)}{N} \quad (7)$$

$$\text{RPD} = \frac{SD\,(y_i^{ref} : y_{i+1}^{ref})}{RMSEP} \quad (8)$$

where N: is the number of samples; R: is the number of PLS factors; y_i^{ref} is the reference value for sample i; y_i is the predicted value for sample i.

● Selection of optimal wavelengths

Spectral wavelengths in hyperspectral images are characterized by their large degree of dimensionality with collinearity and redundancy. Researchers are often interested in finding most important wavelengths which contribute to the evaluation of quality parameters and eliminate wavelengths having no discrimination power. After proving the good performance of the PLS models on predicting the chemical references, the next step was to select only the wavelengths that showed the maximum spectral information.

The regression coefficients (RC), also called β-coefficients, and the Variable Importance in Projection (VIP) scores, were applied to select the most informative optimal wavelengths corresponding to the best full-spectrum PLS calibration model with full spectral variables. The wavelengths that corresponded to the highest absolute values of β-coefficients were considered optimal wavelengths [44]. Based on the studies conducted by Olah et al. [45], all wavelengths at which the VIP scores were above a threshold of 1.0 (highly influential) were selected and compared with those identified using β-coefficients. In this study, only the wavelength with highest β-coefficient (absolute values) from one side and highest VIP scores (above the threshold of 1.0) on another side were selected to establish Multiple Linear Regression (MLR) models, instead of using the whole spectral range. Moreover, all the wavelengths with VIP score above 1 (spectral windows) were also used to improve the performance of PLS regression models.

2.6.4 Statistical analyses

One way ANOVA on quality attributes of table grapes was performed with XLSTAT 2019.1 software (Addinsoft, France). Mean values were separated with Tukey's test ($p<0.05$) to present the significant differences between varieties.

3. Results

3.1. Grape composition

Berries from each grape variety were characterized from their sugar content (Soluble solid content SSC), their Total Flavonoid content (TF) and Total Anthocyanin content (TA) for red varieties only. Table 1 shows that the selected varieties had different total flavonoid content, from 201 mg kg^{-1} FM for Victoria grapes to 1642 mg kg^{-1} FM for Lival grapes, white grapes presenting the lowest phenolic concentration as expected. That agrees with Mikulic-Petkousek et al. [46] which showed that Victoria grapes were among the lower total phenolic content varieties. Similarly, a large range of total anthocyanin content was observed from 217 mg kg^{-1} FM for Alphonse Lavallée to 590 mg kg^{-1} FM for Sable seedless. Their sugar concentration was between 14.0 g/100g (Victoria) to 24.8 g/100g (Alphonse Lavallée) corresponding to ripening level [2]. Statistics showed that TF, TA and SSC were significantly dependent on the grape cultivar.

Table 1. Grape composition. Total Anthocyanins (TA), Total Flavonoids (TF), and Soluble Solid Content (SSC) of table grapes. $^{a\,b\,c\,\&\,d}$ letters within the same column indicate significant differences among table grape cultivars according to Tukey-b test ($p<0.05$). FM: fresh matter.

Grape cultivars	Origin	TF (mg kg^{-1} FM)	TA (mg kg^{-1} FM)	SSC (g $100g^{-1}$)
Sable Seedless	South Africa	1131 ± 267 ^{c}	590 ± 163 ^{a}	19.0 ± 1.8 ^{b}
Alphonse Lavallée	South Africa	829 ± 153 ^{d}	217 ± 61 ^{c}	24.8 ± 1.1^{a}
Lival	France	1642 ± 374 ^{a}	588 ± 222 ^{a}	15.0 ± 1.7^{cd}
Black Magic	Italy	1279 ± 259 ^{b}	399 ± 132 ^{b}	15.4 ± 0.9^{c}
Sugarone Superior Seedless	South Africa	162 ± 43^{e}	0	14.7 ± 1.0 ^{d}
Thompson Seedless	Egypt	826 ± 136 ^{d}	0	15.5 ± 1.9 ^{c}
Victoria	Italy	201 ± 28^{e}	0	14.0 ± 1.5^{e}
		P<0.001	P<0.001	P<0.001

3.2. Spectral profiles

The mean reflectance spectra profile of each grape variety is presented in Figure 2. These spectra obtained by HIS showed clear differences between the grape varieties, as already reported by Baiano et al. [47] on 7 other varieties. White grapes exhibited important reflectance from about 500 to 650 nm on the contrary of reds. Chlorophyll pigments absorb indeed around 540 nm giving the green-yellow color to these varieties as hypothesized by dos Santos et al. (2019). All grapes presented much higher reflectance percentage between 700 and 950 nm, with a mix of intensity between reds and whites but varieties showed similar trends depending on the variety color: whites had higher intensity around 700-720 nm which decreased to 950 nm; reds showed flattened bell curve with a maximum around 820 nm. Absorption band at 840 nm is mainly due to sugar [47] and more than 960 nm to water [48, 49].

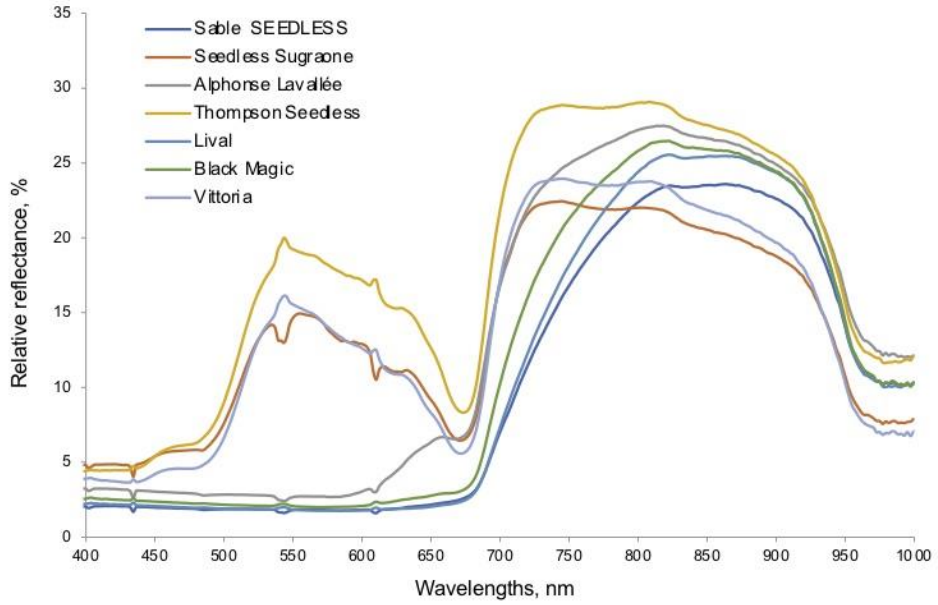

Figure 2. Mean reflectance spectra profiles obtained by hyperspectral imaging spectroscopy. Sable Seedless (dark blue), Seedless Sugraone (red), Alphonse Lavallée (green), Thompson Seedless (purple), Lival (turquoise), Black Magic (orange) and Vittoria (clear blue) table grapes samples.

3.3 Modelisation of table grape composition using the whole spectral range of 411 – 1000 nm

PLSR were developed to establish the relationship between the spectral data extracted from the ROI of the samples and the corresponding TA, TF and SCC content analyzed by conventional chemical method. The whole dataset was employed to select the best pre-treatment for each quality parameter. The results of the models obtained for each quality attribute are reported in Table 2. To select the pre-treatment generating the best model, over the R^2 evaluation, 4 parameters were considered: LVs, RMSE and Bias, which have to be minimized, and RPD, which has to be maximized [48]. All determination coefficients (R^2_{cal} and R^2_{val}) were upper than 0.89 (Table 2) showing that modelising total flavonoids, total anthocyanins and sugar content from HIS data was relevant [49]. Thus, for the modelisation of TF, the best pre-treatments were SNV and WB using 9 and 12 LVs, respectively. The SNV pre-treatment and raw data without pre-treatment (RD) leading to R^2_{cal} = 0.9423; R^2_{val} = 0.9326 with RMSEP = 144.9 mg/kg and R^2_{cal} = 0.9451; R^2_{val} = 0.9351 with RMSEP = 142.0 mg kg^{-1}, respectively. For Total Anthocyanins, the best model was obtained from the SNV data pre-treatment with 3 components only. TA content was predicted with R^2_{cal} = 0.9419 and R^2_{cal} = 0.9457 and RMSEP = 54.2 mg/kg. The best model for SSC was obtained using RD and SNV pre-treatments. The RD pre-treatment, thanks to 15 latent variables, generated a R^2_{cal} =0.9671 and a R^2_{val} = 0.9313 with RMSEP = 1.02 g/100g, while the SNV, using 10 LVs, showed a R^2_{cal} = 0.9472 and a R^2_{val} = 0.9292 with RMSEP = 1.03 g/100g. As for residual prediction deviation (RPD), both SNV and RD pre-treatments generated values close to 4, that suggest the capability of the models to provide a good quantification and satisfactory prediction of TF, TA and SSC [50, 51].The relatively low number of LVs of the models generated by SNV pre-treatment, compared to the others, and the fact that the models were built using grape berries of seven different cultivar contributed to the robustness of the models. And according to the results, the SNV mathematical pre-treatment was selected for predicting quality attributes in table grapes. In order to go further, measured data versus predicted data were plotted for the three models selected (Figure 3). These graphs validated the selected models proving the ability of hyperspectral imaging data to predict TF, TA and SSC in table grapes.

Table 2. Performance of PLS models depending on data pre-treatments for predicting TF, TA and SSC, using full spectra (400-1000 nm). TF: Total Flavonoids, TA: Total Anthocyanins and SSC: Solid Soluble Content. RD: row data, der: derivative, SNV: Standard Normal Variate. LVs: number of latent variables.

Variable	Pre-treat-ment	LVs	Calibration Set		Validation Set			
			R^2_c	RMSEC	R^2_{val}	RMSEP	Bias	RPD
TF	*SNV*	9	0.9423	134.6	0.9326	144.9	9.37	3.85
TF	*1st DER*	9	0.9505	121.2	0.9208	156.7	3.81	3.56
TF	*WB*	12	0.9451	132.1	0.9351	142.0	8.09	3.93
TF	*2nd DER*	5	0.9298	147.0	0.9188	158.9	13.72	3.51
TA	*SNV*	3	0.9419	53.1	0.9457	54.2	17.36	4.05
TA	*1st DER*	4	0.9314	57.9	0.9211	63.6	10.44	3.45
TA	*WB*	6	0.9275	60.1	0.9209	63.5	11.53	3.46
TA	*2nd DER*	4	0.9169	63.8	0.8942	74.6	9.38	2.94
SSC	*SNV*	10	0.9472	0.92	0.9292	1.03	0.01	3.77
SSC	*1st DER*	6	0.9334	1.02	0.9118	1.16	0.06	3.35
SSC	*WB*	15	0.9671	0.73	0.9313	1.02	0.01	3.81
SSC	*2nd DER*	5	0.9110	1.18	0.8897	1.29	0.08	3.01

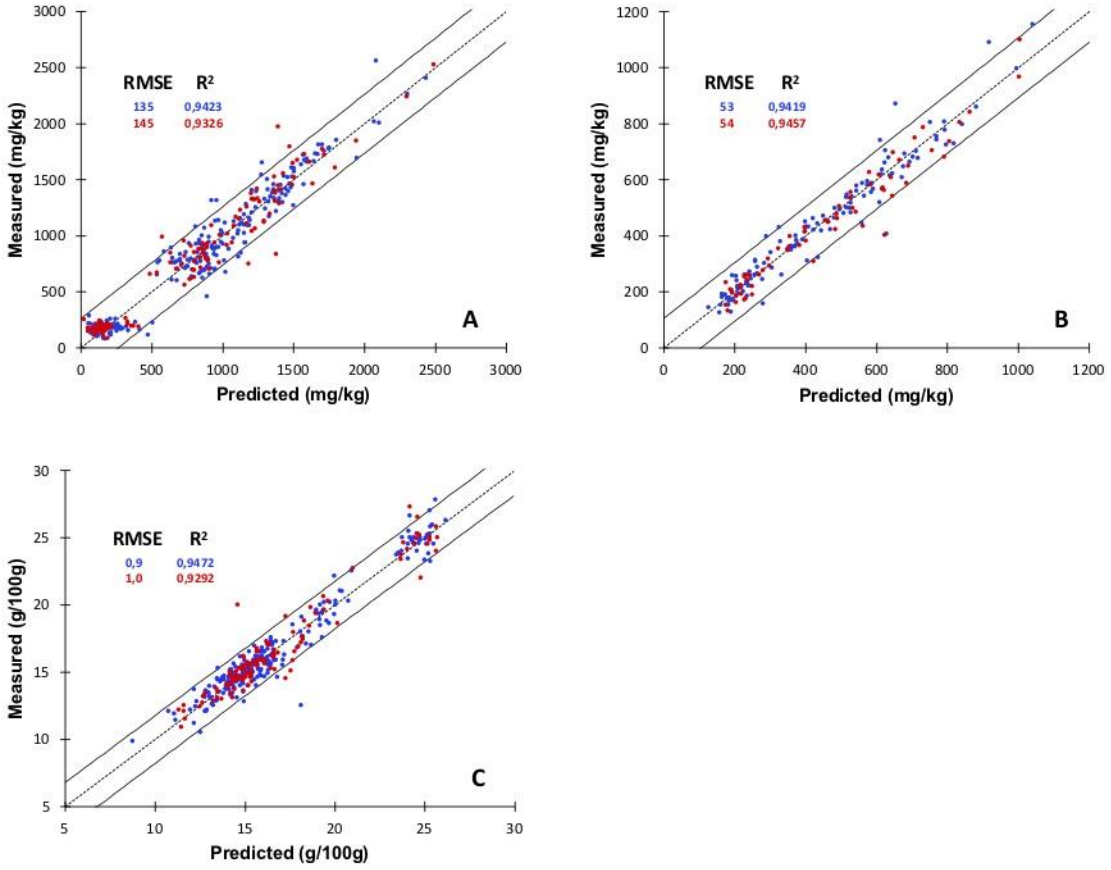

Figure 3. Performance of PLS model using the spectral data pre-treated by SNV. Calibration and external validation for total flavonoids using nine factors (A), for Total Anthocyanins using three factors (B) and for solid soluble content using ten factors (C). Blue dots indicate calibration set and red dots represent predicted set. R^2: determination coefficient, RMSE: root mean squared error.

3.4 Modelisation of table grape composition from optimal wavelengths obtained by β-coefficients

Hyperspectral data with hundreds of contiguous wavelengths for each pixel of image is a great issue for data processing. Therefore, the selection of optimal wavelengths is very important to reduce the computation time, to simplify the prediction model and further to satisfy the real-time inspection [52]. In this section, regression coefficients (RC) resulting from full-spectrum PLS models, were employed to select the key wavelengths aiming to establish the Multiple Linear Regression (MLR) models. Figure 4 shows the values of β-coefficients for the variables Total Flavonoids, Total Anthocyanins and SSC from the HIS data. The optimal wavelengths are those having the highest absolute values of β-coefficients (framed in the figure). Thus 17 specific wavelengths were selected for TF: 434.3; 485.5; 501.9; 543.4; 608.2; 631.4; 648.3; 675.9; 688.7; 707.9; 779; 792; 805; 807.2; 829; 905; and 945.9 nm; 8 for TA: 434.3; 543.4; 604; 616.6; 669.5; 796.3; 943.6 and 952.5 nm; and 23 for SSC: 418; 434.3; 485; 501.9; 539.2; 543.4; 585.1; 646.2; 661; 678; 697.2; 716.5; 792; 802; 805; 807.2; 829; 833; 905.9; 910.3; 939.2; 945.9 and 952.5 nm. Table 3 presents the accuracy and robustness of RC-MLR models built using the selected wavelengths for the prediction of chemical references. The model for the prediction of TF showed R^2 = 0.9525 and 0.9305 for the calibration and validation set respectively and RMSEP = 147.5 mg/kg. For TA, the model had R^2 of 0.9429 and 0.9490 for the calibration and the validation set respectively with RMSEP = 52.0 mg/kg and the model for predicting SSC presented a value of R^2 = 0.9504 and 0.9257 for the calibration and the validation set respectively, and RMSEP = 1.06 g/100g. To visualize these models, measured data vs predicted data was plotted (Figure 5). The correlation between the spectra data and the Total Flavonoid content (R^2_{val} = 0.9305,

Figure 5A), that of Total Anthocyanin content (R^2_{val} = 0.9490, Figure 5B), and that of SSC (R^2_{val} = 0.9257, Figure 5C) were good with points concentrated on the line y=x and narrow scattering of data showing the low error of the model. Thus, our models for TF, TA and SSC showed good quantification and good prediction potential due to their RER and RPD values (Table 3) [49, 50, 51]. However, the values of Bias are rather important for TF and TA but that could be improved. Although the elimination of variables was approximately 92.0%, the MLR model had higher performance in prediction in terms of RMSE and determination coefficient compared to full-spectrum PLSR models. This is attributed to the fact that MLR models only use the optimal wavelengths and neglect unnecessary wavelengths, mitigating the problems of collinearity and overfitting [53]. Therefore, it could be demonstrated that RC algorithm is useful and effective for the selection of key wavelengths in predicting TF, TA and solid soluble content in table grape.

Table 3. MLR model performance for Total Flavonoids (TF), Total Anthocyanins (TA) and Solid Soluble Content (SSC) from optimal wavelengths selection based on◎◎◎coefficient of the best PLS full spectra analysis.

Variable	Optimal wavelengths (nm)	Calibration Set		Validation Set			
		R^2_c	RMSEC	R^2_{val}	RMSEP	Bias	RPD
TF	434.3; 485.5; 501.9; 543.4; 608.2; 631.4; 648.3; 675.9; 688.7; 707.9; 779; 792; 805; 807.2; 829; 905; 945.9	0.9525	119.5	0.9305	147.5	12.66	3.78
TA	434.3; 543.4; 604; 616.6; 669.5; 796.3; 943.6; 952.5	0.9429	52.0	0.9490	52.0	14.31	4.22
SSC	418; 434.3; 485; 501.9; 539.2; 543.4; 585.1; 646.2; 661; 678; 697.2; 716.5; 792; 802; 805; 807.2; 829; 833; 905.9; 910.3; 939.2; 945.9; 952.5	0.9504	0.87	0.9257	1.06	-0.05	3.68

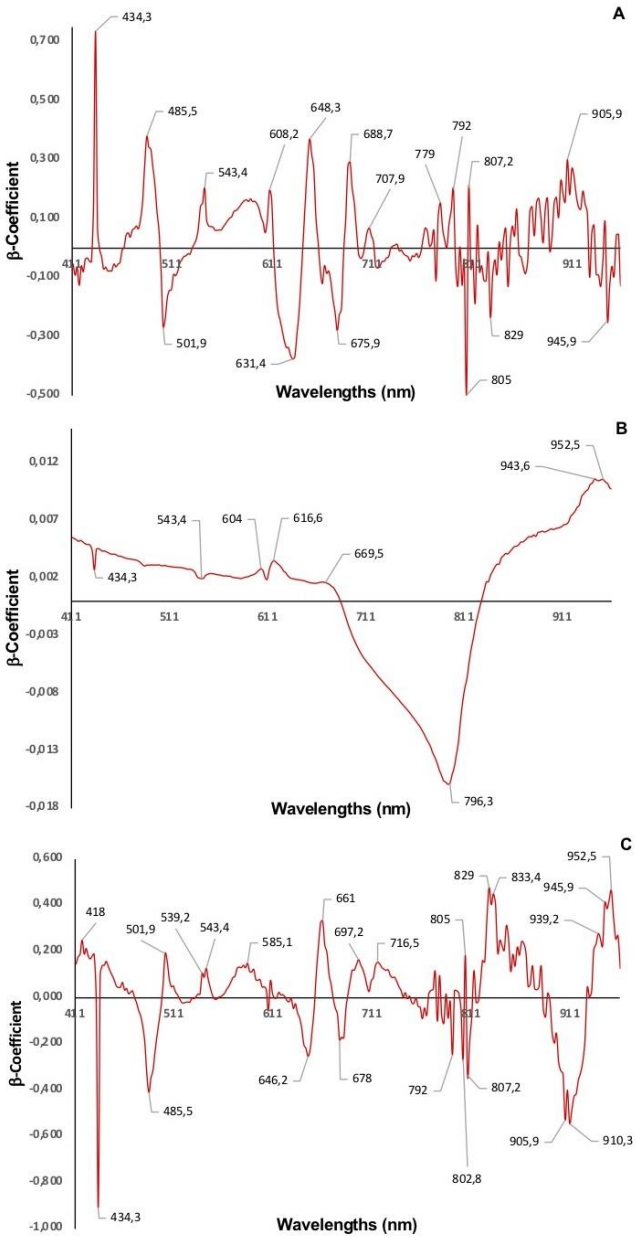

Figure 4. Values of β-coefficients for all wavelengths for predicting quality attributes in table grape for the variable, Total Flavonoids (A), Total Anthocyanins (B) and Sugar content SSC (C).

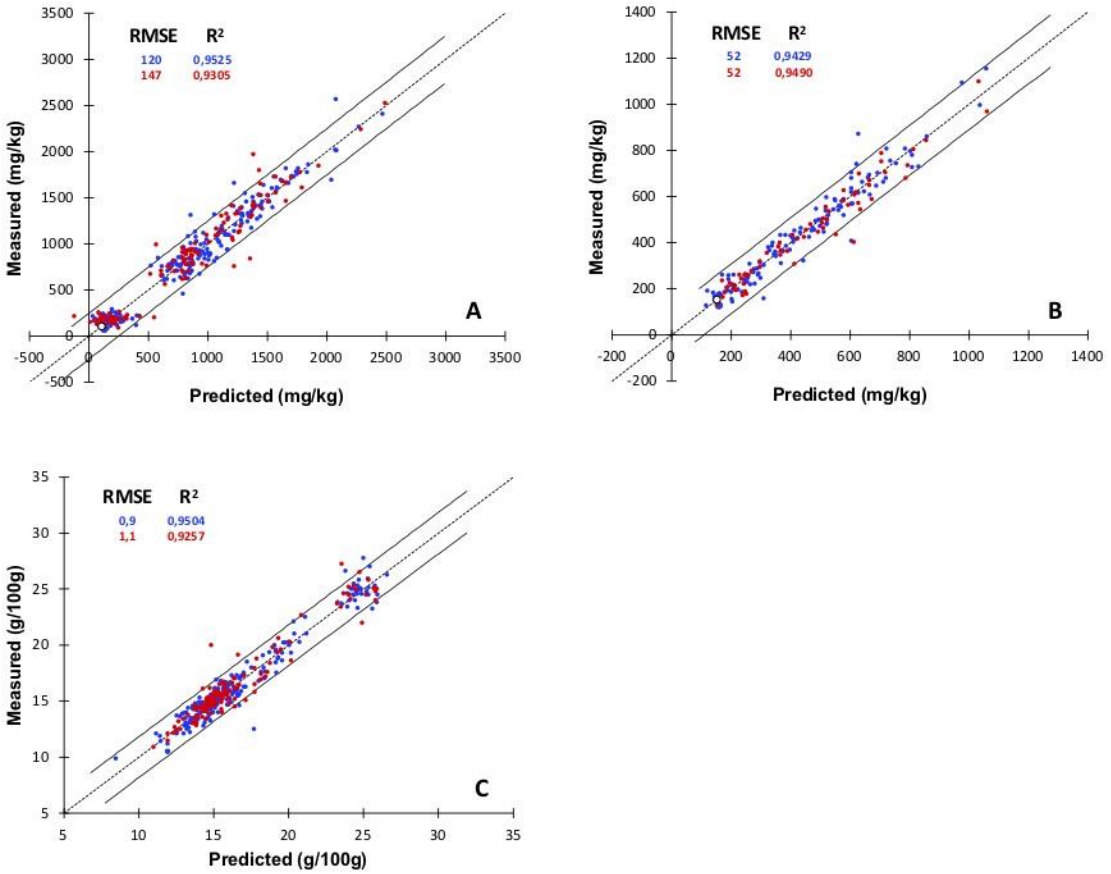

Figure 5. Performance of MLR models using only the optimal wavelengths extracted from β-coefficients of PLS analysis. Calibration and external validation using SNV pre-treated data: (A) for Total Flavonoids, (B) for Total Anthocyanins and (C) for SSC. Blue dots indicate calibration set and red dots represent predicted set.

3.5. Modelisation of table grape composition from optimal wavelengths obtained by VIPs score

The VIP scores resulting from the best preprocessing PLS regression model were used to develop a robust model by selection of feature-related wavelengths for TF, TA and SSC of table grapes. The performance of the developed model by MLR depended largely on the cut-off value of the VIP scores. Generally, the "greater-than-one" rule is used to identified optimal wavelengths [54]. Only the wavelengths with highest value of VIP scores, above the threshold of 1.0, were selected to establish MLR models, whereas the wavelengths with VIP scores above 1 (spectral windows) were selected to improve PLS model performance. As shows Figure 6 the optimal wavebands selected from all 283 wavebands were ten (434.3; 543.4; 610.3; 633.5; 697.2; 781.1; 785.5; 805; 905.9 and 910.3 nm), three (710; 785.5 and 943.6 nm) and eight (434.3; 501.9; 543.4; 610.3; 656.8; 686.5; 802.8 and 809.4 nm) for TF, TA and SSC, respectively. Table 4 presents the accuracy and robustness of MLR models for the prediction of TF, TF and SSC based on VIP score. The model for the variable TF leading to R^2 of 0.9032 and 0.8971 respectively for the calibration and the validation set and with RMSEP = 178.3 mg/kg. The model for predicting TA content showed R^2 of 0.9374 and 0.9432 respectively for the calibration and the validation set with RMSEP = 55.1 mg/kg. For the sugar content (SSC), the VIPs-MLR model had R^2 equal to 0.8689 and 0.8277 for the calibration and the validation sets respectively with RMSEP = 1.61 g/100g. The MLR models based on the VIPs wavelengths selection showed values of RPD close or higher to 2.5, which indicated that these models were good enough to have a high utility value model [52]. However, these results showed a declined prediction accuracy of TF and SSC models comparing to the prediction ability of full-spectrum PLSR and RC-MLR models. Once more, to check the quality of the models, the measured data vs predicted

data was plotted (Figure 7). All graphs showed that predicted data fitted with measured data. The model is particularly good for TA with more narrow spread of the data.

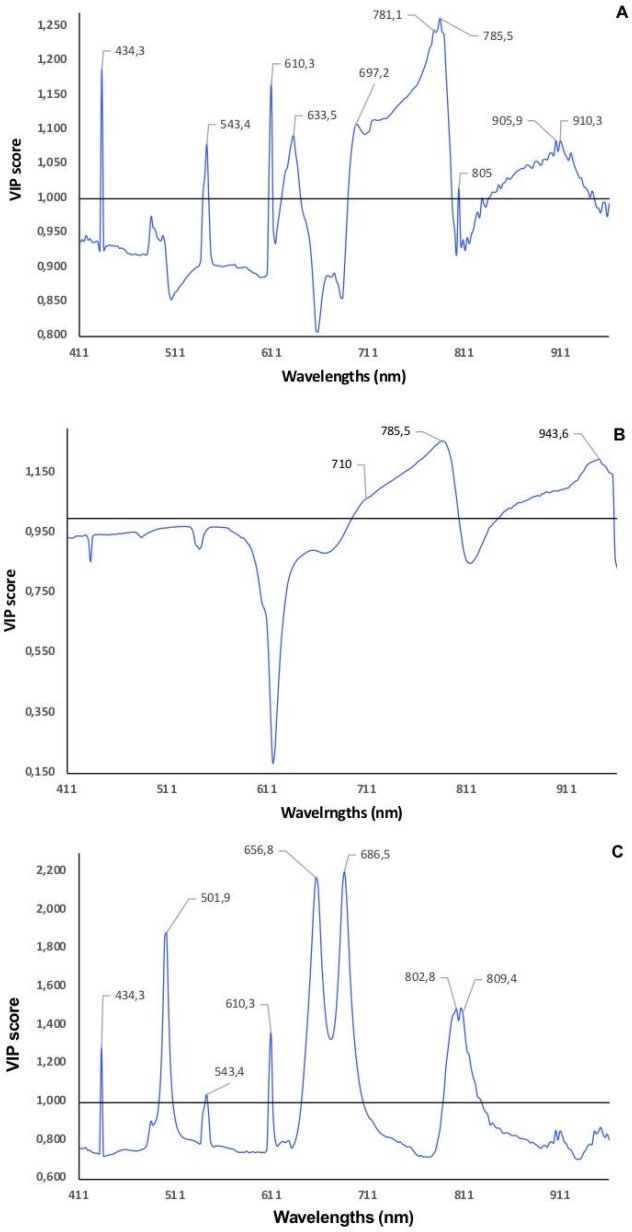

Figure 6. Values of VIP scores for all wavelengths for predicting quality attributes in table grape for the variable, Total Flavonoids (A), Total Anthocyanins (B) and Sugar content SSC (C).

Table 4. Performance of MLR models for predicting Total Flavonoids (TF), Total Anthocyanins (TA) and the Solid Soluble Content (SSC) using the optimal wavelengths extracted from VIPs (Variable Importance in the Projection) of the best PLS full spectra analysis.

Variable	Optimal wavelengths (nm)	Calibration Set		Validation set			
		R^2_c	RMSEC	R^2_{val}	RMSEP	Bias	RPD
TF	434.3; 543.4; 610.3; 633.5; 697.2; 781.1; 785.5; 805; 905.9; 910.3	0.9032	170.7	0.8971	178.3	-7.16	3.13
TA	710; 785.5; 943.6	0.9374	54.5	0.9432	55.1	17.27	3.98

Brix°	434.3; 501.9; 543.4; 610.3; 656.8; 686.5; 802.8; 809.4	0.8689	1.41	0.8277	1.61	-0.03	2.41

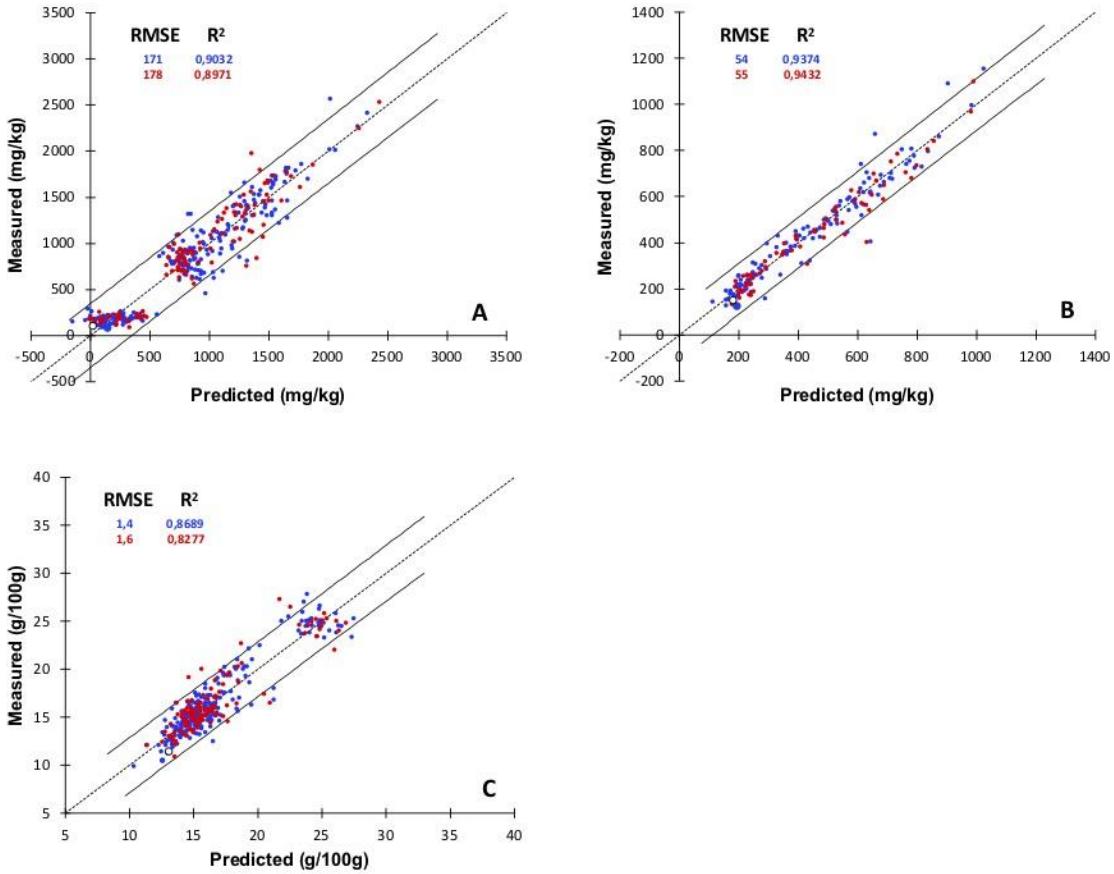

Figure 7. Performance of MLR model using the optimal wavelengths extracted from VIPs score of the best full-spectrum PLS analysis. Calibration and external validation from SNV pre-treated data for (A) Total Flavonoids, (B) Total Anthocyanins and (C) Solid Soluble Content. Blue dots indicate calibration set and red dots represent predicted set.

The last trial was to select all the wavelengths with VIP score above 1 (spectral windows). New VIPs-PLS models were then build (Table 5). The VIPs-PLS model to predict TF (spectral windows: 434.3; 539.2 - 543.4; 608.2 - 610.3; 620.8 - 639.8; 690.8 - 796.3; 829 and 835.5 - 943.6 nm) generated a $R^2cal = 0.9560$, $R^2val = 0.9438$ and RMSEP = 131.8 mg/kg, using 14 LVs. The model for predicting TA content (spectral windows: 697.2 - 802.8 and 842.1 - 957 nm) was fed by 8 LVs, and generated $R^2cal = 0.9617$, $R^2val = 0.9480$ and RMSEP = 52.8 mg/kg. For SSC (spectral windows: 420.1; 424.1; 428.2 - 432.3; 436.3; 479.3 - 481.4; 535.1 - 541.3; 545.4; 555.9; 560; 564.2; 585.1 - 639.8; 673.8 - 688.7; 716.5 - 720.8; 864; 881.6; 890.5 - 892.7; 899.3; 912.5 - 914.8; 921.4 - 934.7; 939.2 and 954.8 – 957 nm), the VIPs-PLR model leading to $R^2_{cal} = 0.9360$, $R^2_{val} = 0.9134$ and RMSEP = 1.14 g/100g, using 14 LVs. RPD values suggested that all three models were good enough to quantify and predict the corresponding TF, TA and SSC values [55]. Figure 8 shows the curves measured data vs predicted data for these best models. Again, the models fitted well with the measured data since the data spread is rather narrow for all three parameters, suggesting good prediction models from specific windows HIS data. The simplified VIPs-PLSR model performed slightly

increase prediction accuracy of TF and TA comparing to the prediction ability of full-spectrum PLSR models, in term of determination coefficient, RMSE and RPD values. However, the best prediction model for SSC was built using the whole spectral data.

Table 5. Performance of PLS models for predicting Total Flavonoids (TF), Total Anthocyanins (TA) and the sugar content (SSC) using only the optimal wavelengths windows extracted from VIPs (Variable Importance in the Projection) of PLS full spectra analysis.

Variable	Spectral windows (nm)	No. LVs	Calibration Set		Validation Set			
			R^2_c	RMSEC	R^2_{val}	RMSEP	Bias	RPD
TF	434.3; 539.2 - 543.4; 608.2 - 610.3; 620.8 - 639.8; 690.8 - 796.3; 829; 835.5 - 943.6	14	0..9560	118.9	0.9438	131.8	-6.44	4.23
TA	697.2 - 802.8; 842.1 - 957	8	0.9617	44.1	0.9480	52.8	13.30	4.16
Brix°	420.1; 424.1; 428.2 - 432.3; 436.3; 479.3 - 481.4; 535.1 - 541.3; 545.4; 555.9; 560; 564.2; 585.1 - 639.8; 673.8 - 688.7; 716.5 - 720.8; 864; 881.6; 890.5 - 892.7; 899.3; 912.5 - 914.8; 921.4 - 934.7; 939.2; 954.8 - 957	14	0.9360	1.02	0.9134	1.14	-0.05	3.40

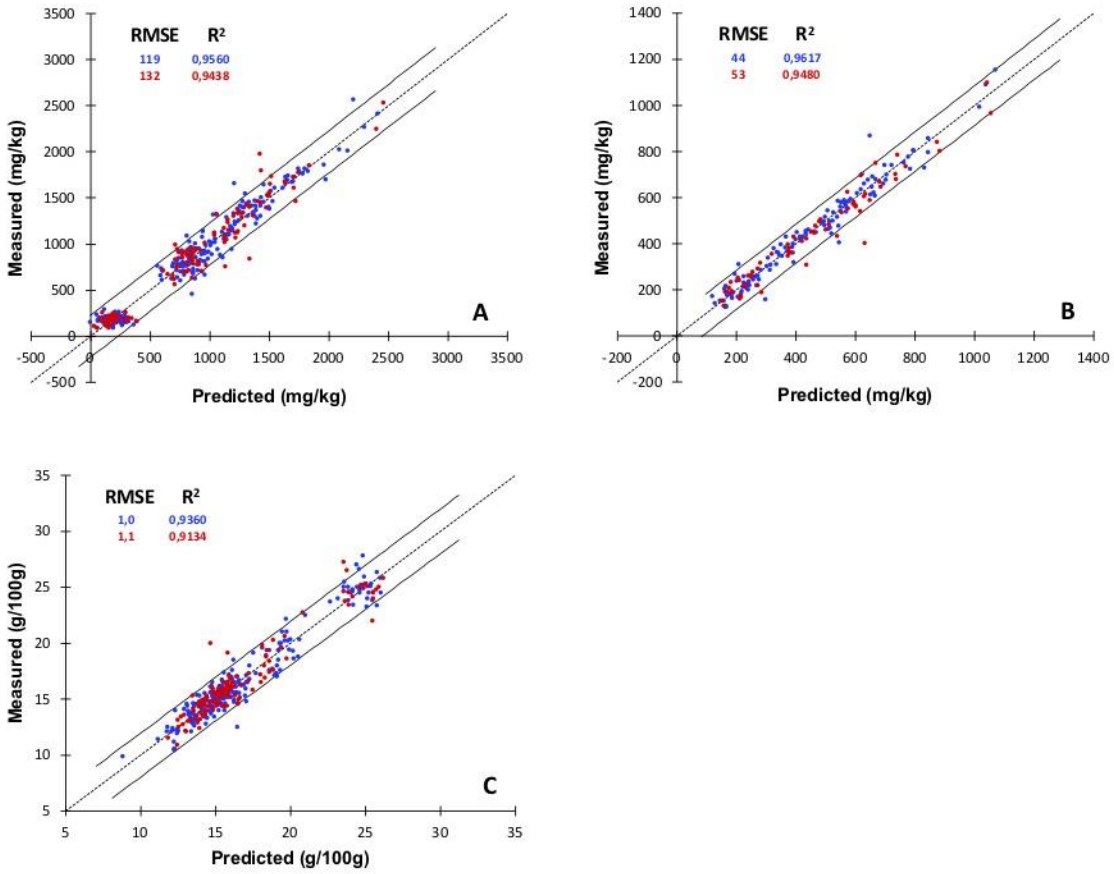

Figure 8. Performance of PLS model using the optimal wavelength windows extracted from VIPs score (> 1) of PLS analysis. Calibration and external validation for (A) Total Flavonoids, (B) Total

Anthocyanins and (C) Solid Soluble Content. Blue dots indicate calibration set and red dots represent predicted set.

4. Discussion

The possibility to use the full spectra from HIS to generate a relevant PLS-model to predict the sugar content was indeed reported by Baiano et al. [47] using the same device. These authors developed a calibration models able to predict SSC of white and red table grape with R^2_{val} of 0.94 and 0.93, respectively. Our method was however valid for all grape varieties, with all reds and whites, which would be easier to manage in an industrial point of view. In addition, the results of the present study were comparable to those of another work carried out by Gomes et al. [56], in which the prediction of SSC in wine grape was performed using two different model development techniques i.e., PLS regression and Neural Networks. The obtained values of R^2 of prediction were 0.92 for both PLS regression and Neural Networks with RMSEP of 0.94°Brix and 0.96°Brix, respectively. Hence, a good capacity of correlation was achieved in numerous other works on prediction of SSC for table and wine grapes [24, 38, 57, 58].

Other authors have also reported good performance of linear models to predict the total anthocyanin content, with $R^2_{CV} > 0.94$ using spectral data in Vis-NIR [59] and NIR ranges [60] or total phenols content, with $R^2_{CV} = 0.89$ using the spectral data in Vis-NIR range [57, 61]. Moreover, several studies also reported very good performance of nonlinear models to predict the TA content in whole Port and Cabernet sauvignon wine grape using the hyperspectral imaging device in Vis-NIR range [38, 56, 62]. Thus, our results were at least as good at those of other works but for the first time showed the relevance of HIS on red and white table grapes.

Our results highlighted that not only hyperspectral imaging is a relevant method to predict TA, TF and SSC content, but also the reduction of data is possible using MLR method with β-coefficients or variable importance in the projection VIP. RC methods were already reported to be relevant to predict sugar content in the case of lychee fruit [55] and the total polyphenols concentration in cocoa beans [60, 63]. Sen and co-workers [64] have also applied VIP selection to build OPLS models for the prediction of chemical parameters of wine by combined use of visible and mid-infrared (MIR) spectroscopies. These authors have built models able to predict anthocyanin compounds, total phenol content and SSC of red wine with R^2_{val} ranging between 0.77 and 0.96.

The use of VIP in a PLR model (specific windows) were applied by Sen and co-workers [64] to build OPLS models for the prediction of chemical parameters of wine by combined use of visible and mid-infrared (MIR) spectroscopies. These authors have built models able to predict anthocyanin compounds, total phenol content and SSC of red wine with R^2_{val} ranging between 0.77 and 0.96. Our work is thus in adequation with the previous studies and showed for the first time that reducing data thanks to VIP or β-coefficients from HIS is suitable for table grapes. No similar results have been found in table grapes for the control of Total Flavonoids and the Total Anthocyanins, although they have been found in wine grapes and other matrices with errors of the same order of magnitude [24, 59, 60, 65].

Hyperspectral imaging is a tool, which could provide relevant on-line information about Total Flavonoid, Total Anthocyanins and Total Soluble Solid contents through the use of consistent prediction models. The models from the full spectra generated by SNV pre-treatment and the fact that the models were built using grape berries of seven different cultivar contributed to the robust-ness of our models. The possibility to use the same pre-treatment for all parameters and all varieties is interesting and could limit the complexity of the method and avoid mistakes in a professional use.

The reduction of data using only the wavelength with highest β-coefficient (absolute values) from one side, and spectral windows obtained from all the wavelengths with VIPs > 1 on another side, would allow an industrial use needing less computer data memory

and quicker answers. That method could be used also as quality control. Database has first to be expanded not only to strength our current models but also to test new non-linear models. Another step would be to implement hyperspectral imaging on an industrial conveyor belt to take into accounts elements such as vibration on the conveyor but also analytical speed to provide real time information. Nonetheless, that tool could anyway be used for a rapid table grape characterization in producer or industry places.

Author Contributions: Conceptualization, M. Gabrielli; methodology, M. Gabrielli and P. Picouet; validation, P. Picouet; formal analysis, M. Gabrielli; investigation, V. Lançon-Verdier, M. Gabrielli and C. Maury; resources, V. Lançon-Verdier; data curation, M. Gabrielli; writing—original draft preparation, M. Gabrielli and C. Maury; writing—review and editing, C. Maury, M. Gabrielli and P. Picouet; visualization, C. Maury; supervision, C. Maury; project administration, C. Maury; funding acquisition, C. Maury. All authors have read and agreed to the published version of the manuscript.

Funding: This research was conducted in the framework of the regional program "Objectif Végétal, Research, Education and Innovation in Pays de la Loire", supported by the French Region Pays de la Loire, Angers Loire Métropole and the European Regional Development Fund. The chemiometry was realized thanks to Region Pays de la Loire and Interprofession des Vins du Val de Loire Inter-Loire in the frame of the O3VINS project.

Institutional Review Board Statement: Not applicable.

Informed Consent Statement: Not applicable.

Data Availability Statement: Data are available in section "MDPI Research Data Policies" at https://www.mdpi.com/ethics.

Acknowledgments: In this section, you can acknowledge any support given which is not covered by the author contribution or funding sections. This may include administrative and technical support, or donations in kind (e.g., materials used for experiments).

Conflicts of Interest: The authors declare no conflict of interest. The funders had no role in the design of the study; in the collection, analyses, or interpretation of data; in the writing of the manuscript, or in the decision to publish the results.

References

1. OIV (International Organisation of Vine and Wine). **2019**. Statistical Report on world vitiviniculture. Available on line: http://www.oiv.int/public/medias/6782/oiv-2019-statistical-report-on-world-vitiviniculture.pdf (accessed on 12/01/2021)
2. Valero, D.; Valverde, J.; Martíınez-Romero, D.; Guillén, F.; Castillo, S.; Serrano, M. The combination of modified atmosphere packaging with eugenol or thymol to maintain quality, safety and functional properties of table grapes. *Postharvest Biol. Technol.* **2006**, *41*, 317–327. https://doi.org/10.1016/j.postharvbio.2006.04.011
3. Hellín, P.; Manso, A.; Flores, P.; Fenoll, J. Evolution of aroma and phenolic compounds during ripening of 'Superior seedless' grapes. *J. Agric. Food Chem.* **2010**, *58*(10), 6334–6340. https://doi.org/10.1021/jf100448k
4. Zeppa, G.; Rolle, L.; Gerbi, V. Valutazione mediante consumer test dell'attitudine al consumo diretto di un'uva a bacca rossa. *Indus. Alim.* **1999,** *38*, 818-24.
5. Piva, C.R.; López Garcia, J.J.; Morgan, W. The ideal table grapes for the Spanish market. *Rev. Brasil. Frutic.* **2006**, *28*, 258–261. https://doi.org/10.1590/S0100-29452006000200023
6. Abdullah, M.Z.; Guan, L.C.; Lim, K.C.; Karim, A.A. The applications of computer vision system and tomographic radar imaging for assessing physical properties of food. *J. Food Eng*. **2001**, *61*, 125–135. https://doi.org/10.1016/S0260-8774(03)00194-8
7. Turati, F.; Rossi, M.; Pelucchi, C.; Levi, F.; La Vecchia, C. Fruit and vegetables and cancer risk: a review of southern European studies. *Br. J. Nutr.* **2015**, *113*, S102–S110.

8. Vieira, A.R.; Abar, L.; Vingeliene, S.; Chan, D.S.M.; Aune, D.; Navarro-Rosenblatt, D.; Stevens, C.; Greenwood, D.; Norat, D. Fruits, vegetables and lung cancer risk: a systematic review and meta-analysis. *Ann. Oncol*., **2016**, *27*, 81–96. https://doi.org/10.1093/annonc/mdv381
9. Perestrelo, R.; Silva, C.; Pereira, J.; Câmara, J.S. Healthy effects of bioactive metabolites from *Vitis vinifera* L. grapes: A review. In *Grapes: Production, phenolic composition and potential biomedical effects*, Câmara, J.S. Ed. Publisher: Nova Science Technology **2014**, 305–338.
10. Shahidi, F.; Ambigaipalan, P. Phenolics and polyphenolics in foods, beverages and spices: Antioxidant activity and health effects – A review. *J. Funct. Foods* **2015**, *18*, 820 – 897. https://doi.org/10.1016/j.jff.2015.06.018
11. Basile, T.; Alba, V.; Gentilesco, G.; Savino, M.; Tarricone, L. Anthocyanins pattern variation in relation to thinning and girdling in commercial Sugrathirteen® table grape. *Sci. Hortic*. **2018**, *227*, 202–206. https://doi.org/10.1016/j.scienta.2017.09.045
12. Río Segade, S.; Giacosa, S.; Torchio, F.; Laura de Palma, L.; Novello, V.; Gerbi, V.; Rolle, L. Impact of different advanced ripening stages on berry texture properties of 'Red Globe' and 'Crimson Seedless' table grape cultivars (*Vitis vinifera* L.). *Sci. Hortic*. **2013**, *160*, 313–319. https://doi.org/10.1016/j.scienta.2013.06.017
13. Kontoudakis, N.; Esteruelas, M.; Fort, F.; Canals, J. M.; Zamora, F. Comparison of methods for estimating phenolic maturity in grapes: correlation between predicted and obtained parameters. *Anal. Chim. Acta* **2009**, *660*, 127-133. https://doi.org/10.1016/j.aca.2009.10.067
14. Mota, A.; Pinto, J.; Fartouce, I.; Correia, M.J; Costa, R.; Carvalho, R.; Aires, A.; Oliveira, A.A. Chemical profile and antioxidant potential of four table grape (*Vitis vinifera*) cultivars grown in Douro region, Portugal. *Ciência Téc. Vitiv*. **2018**, *33*(2) 125-135. https://doi.org/10.1051/ctv/20183302125
15. Zhao, Y.; Zhang, C.; Zhu, S.; Gao, P.; Feng, L.; He, Y. Nondestructive and rapid variety discrimination and visualization of single grape seed using near-infrared hyperspectral imaging technique and multivariate analysis. *Molecules*, 23, *6*, 1352. https://doi.org/10.3390/molecules23061352
16. Fragoso, S.; Mestres, M.; Busto, O.; Guasch J. Comparison of three extraction methods used to evaluate phenolic ripening in red grapes. *J. Agric. Food Chem*. **2010**, *58*, 4071e4076. https://doi.org/10.1021/jf9040639
17. Costa, G.; Noferini, M.; Fiori, G.; Torrigiani, P. Use of vis/nir spectroscopy to assess fruit ripening stage and improve management in post-harvest chain. Fresh Prod. 2009, 3, 35–41.
18. Arendse, E.; Fawole, O.A.; Magwaza, L.S.; Opara, U.L. Non-destructive prediction of internal and external quality attributes of fruit with thick rind: A review. *J. Food Eng*. **2018**, 217, 11-23. https://doi.org/10.1016/j.jfoodeng.2017.08.009
19. Whitacre, E.; Oliver, J.; Van Den Broek, R.; Van Engelen, P.; Remers, B.K.; Van der Horst, B.; Stewart, A.M.; Jansen-Beuvink, A. Predictive analysis of cocoa procyanidins using near-infrared spectroscopy techniques. *J. Food Sci*. **2003**, *68*, 2618-2622. https://doi.org/10.1111/j.1365-2621.2003.tb05779.x
20. Chen, Q.; Zhao, J.; Lui, M.; Cai, J.; Lui, J. Determination of total polyphenols content in green tea using FT-NIR spectroscopy and different PLS algorithms. *J. Pharm. Biomed. Anal*. **2008**, 46, 568–573. https://doi.org/10.1016/j.jpba.2007.10.031
21. Cozzolino, D; Kwiatkowski, M.J.; Parker, M.; Cynkar, W.U.; Dambergs, R.G.; Gishen, M.; Herderich, M.J. Prediction of phenolic compounds in red wine fermentations by visible and near infrared spectroscopy. *Anal. Chim. Acta* **2004**, 513, 73–80.
22. Versari, A.; Parpinello, G.P.; Mattioli, A.U.; Galassi, S. Determination of grape quality at harvest using Fourier-transform mid-infrared spectroscopy and multivariate analysis. *Am. J. Enol. Vitic*. **2008**, *59*, 317-322. https://doi.org/10.1016/j.aca.2003.08.066
23. Cozzolino, D.; Cynkar, W.U.; Dambergs, R.G.; Mercurio, M.D.; Smith, P.A. Measurement of condensed tannins and dry matter in red grape homogenates using near infrared spectroscopy and partial least squares. *J. Agric. Food Chem.* **2008**, *56*, 7631-7636. https://doi.org/10.1021/jf801563z
24. Pathmanaban, P.; Gnanavel, B.K.; Anandan, S.S. Recent application of imaging techniques for fruit quality assessment. *Trends Food Sci. Technol.* **2019**, *94*, 32-42. https://doi.org/10.1016/j.tifs.2019.10.004
25. Ma, J.; Sun, D.W.; Pu, H.; Cheng, J.H.; Wei Q. Advanced techniques for hyperspectral imaging in the food industry: principles and recent applications. *Annu. Rev. Food Sci. Technol*. **2019**, *10*, pp. 197-220. https://doi.org/10.1146/annurev-food-032818-121155

26. Cen, H.; Lu, R.; Ariana, D.P.; Mendoza, F. Hyperspectral imaging-based classification and wavebands selection for internal defect detection of pickling cucumbers. Food Bioproc. Technol. 2013, 7:1689–1700. http://dx.doi.org/10.13031/aim.20131671220
27. Torres, I.; Amigo, J.-M. An overview of regression methods in hyperspectral and multispectral imaging. *Data Handl. Sci. Technol*. **2020**, *32*, 205-230. https://doi.org/10.1016/B978-0-444-63977-6.00010-9
28. Elmasry, G.; Kamruzzaman, M.; Sun, D. W.; Allen, P. Principles and applications of hyperspectral imaging in quality evaluation of agro-food products: A review. *Crit. Rev. Food Sci. Nutr.* **2012**, *52*(11), 999–1023. https://doi.org/10.1080/10408398.2010.543495
29. Qin, J.W.; Kim, M.S.; Chao, K.L.; Chan, D.E.; Delwiche, S.R.; Cho, B.K. Line-scan hyperspectral imaging techniques for food safety and quality applications. *Appl. Sci. Basel.* **2017**, *7*, 125. https://doi.org/10.3390/app7020125
30. Siche, R.; Vejarano, R.; Aredo, V.; Velasquez, L.; Saldaña, E.; Quevedo, R. Evaluation of food quality and safety with hyperspectral imaging (HSI). *Food Eng. Rev*. **2016**, *8*, 306–322. https://doi.org/10.1007/s12393-015-9137-8
31. Wu, D.; Sun, D.-W. Advanced applications of hyperspectral imaging technology for food quality and safety analysis and assessment: a review- Part II: Applications. *Innov. Food Sci. Emerg. Technol.* **2013**, *19*, 15-28. https://doi.org/10.1016/j.ifset.2013.04.016
32. Feng, L.; Zhu, S.; Zhang, C.; Bao, Y.; Gao, P.; He, Y. Variety Identification of Raisins Using Near-Infrared Hyperspectral Imaging. Molecules 2018, 23, 2907. https://doi.org/10.3390/molecules23112907
33. Calvini, R.; Ulrici, A.; Amigo, J.M. Practical comparison of sparse methods for classification of Arabica and Robusta coffee species using near infrared hyperspectral imaging. Chemom. *Intell. Lab. Syst.* **2015**, *146*, 503–511. https://doi.org/10.1016/j.chemolab.2015.07.010
34. Chandrasekaran, I.; Panigrahi, S.S.; Ravikanth, L.; Singh, C.B. Potential of Near-Infrared (NIR) spectroscopy and hyperspectral imaging for quality and safety assessment of fruits: An overview. *Food Anal. Methods* **2019**, 12(11): 2438-2458. https://doi.org/10.1007/s12161-019-01609-1
35. Pu, Y.Y.; Feng, Y.Z.; Sun, D.W. Recent progress of hyperspectral imaging on quality and safety inspection of fruits and vegetables: a review. Compr. *Reviews Food Sci. Food Saf*. **2015**, *14*(2), 176-188. https://doi.org/10.1111/1541-4337.12123
36. Gowen, A.; O'Donnell, C.; Cullen, P.; Downey, G.; Frias, J. Hyperspectral imaging-an emerging process analytical tool for food quality and safety control. *Trends Food Sci. Technol.* **2007**, *18*, 12, 590–598. https://doi.org/10.1016/j.tifs.2007.06.001
37. Taghizadeh, M.; Gowen, A.A.; O'Donnell, C.P. Comparison of hyperspectral imaging with conventional RGB imaging for quality evaluation of *Agaricus bisporus* mushrooms. *Biosyst. Eng*. **2011**, *108*(2), 191–194. https://doi.org/10.1016/j.biosystemseng.2010.10.005
38. Fernandes, A.M.; Franco, C.; Mendes-Ferreira, A.; Mendes-Faia, A.; da Costa, P.L.; Melo-Pinto, P. Brix, pH and anthocyanin content determination in whole Port wine grape berries by hyperspectral imaging and neural networks. *Comput. Electron. Agric*. **2015**, *115*, 88–96. https://doi.org/10.1016/j.compag.2015.05.013
39. Tallada, J.G.; Bato, P.M.; Shrestha, B.P.; Kobayashi, T.; Nagata, M. Quality evaluation of plant products. In *Hyperspectral Imaging Technology in Food and Agriculture*, Park, B.; Lu, R., Eds. Publisher: Springer, New York, NY, **2015,** 227–249.
40. Fracassetti, D.; Gabrielli, M.; Corona, O.; Tirelli, A. Characterisation of Vernaccia Nera (*Vitis vinifera* L.) grapes and wine. *S. Afr. J. Enol. Vitic.* **2017**, *38*, 1, 72-81.
41. Lee, J.; Kang, H. Flood fill mean shift: a robust segmentation algorithm. Int. *J. Control, Autom. Syst*. **2010**, *8*(6), 1313–1319. DOI 10.1007/s12555-010-0617-6
42. Picouet, P.A.; Gou, P.; Hyypiö, R.; Castellari, M. Implementation of NIR technology for at-line rapid detection of sunflower oil adulterated with mineral oil. *J. Food Eng*. **2018**, 230, 18-27. https://doi.org/10.1016/j.jfoodeng.2018.01.011
43. Stchur, P.; Cleveland, F.; Zhou, J.; Michel, R.G. A review of recent application of near infrared spectroscopy and the characterisation of a novel PbS CCD assay based near-infrared spectrometer. *J. Appl. Spect. Rev*. **2002**, *37*, 383-428. https://doi.org/10.1081/ASR-120016293
44. Rajkumar, P.; Wang, N.; EImasry, G.; Raghavan, G.S.V.; Gariepy, Y. Studies on banana fruit quality and maturity stages using hyperspectral imaging. Journal of Food Engineering, *J. Food Eng.* **2012**, 108, 194–200. https://doi.org/10.1016/j.jfoodeng.2011.05.002

45. Olah, M.; Bologa, C.; Oprea, T.I. An automated PLS search for biologically relevant QSAR descriptors. *J. Comp.-Aided Mol. Des.* **2004**, *18*, 437–449. https://doi.org/10.1007/s10822-004-4060-8
46. Mikulic-Petkovsek, M.; Skvarc, A.; Rusjan, D. Biochemical composition of different table grape cultivars produced in Slovenia. *J. Hortic. Sci. Biotechnol*. **2019**, *94*(3), 368-377. https://doi.org/10.1080/14620316.2018.1504629
47. Baiano, A.; Terracone, C.; Peri, G.; Romaniello, R. Application of hyperspectral imaging for prediction of physico-chemical and sensory characteristics of table grapes. *Comput. Electron. Agric.* **2012**, *87*, 142-151. https://doi.org/10.1016/j.compag.2012.06.002
48. dos Santos Costa, D.; Mesa, N.F.O.; Freire, M.S.; Ramos, R.P.; Mederos, B.J.T. Development of predictive models for quality and maturation stage attributes of wine grapes using VIS-NIR reflectance spectroscopy. *Postharvest Biol. Technol.* **2019**, *150*, 166-178. https://doi.org/10.1016/j.postharvbio.2018.12.010
49. Yang, Q.; Sun, D.; Cheng, W. Development of simplified models for nondestructive hyperspectral imaging monitoring of TVB-N contents in cured meat during drying process. *J. Food Eng*. **2017**, *192*, 53– 60. https://doi.org/10.1016/j.jfoodeng.2016.07.015
50. De Marchi, M.; Fagan, C.C.; O'donnell, C.P.; Cecchinato, A.; Dal Zotto, R.; Cassandro, M.; Penasa; Bittante, G. (). Prediction of coagulation properties, titratable acidity, and pH of bovine milk using mid-infrared spectroscopy. *J. Dairy Sci.* **2009**, *92*(1), 423-432.
51. Gherardi Hein, P.R.; Maioli Campos, A.C.; Trugilho, P.F.; Lima, J.T.; Chaix, G. Near infrared spectroscopy for estimating wood basic density in *Eucalyptus urophylla* and *E. grandis*. *Cerne* **2009**, *15*(2), 133-141.
52. Pu, H.; Kamruzzaman, M.; Sun, D. Selection of feature wavelengths for developing multispectral imaging systems for quality, safety and authenticity of muscle foodse. A review. *Trends Food Sci. Technol.* **2015**, *45*, 86-104. https://doi.org/10.1016/j.tifs.2015.05.006
53. Galvão, R.K.H.; Araújo, M.C.U.; Fragoso, W.D.; Silva, E.C.; José, G.E.; Paiva, H.M. A variable elimination method to improve the parsimony of MLR models using the successive projections algorithm. *Chemomet. Intell. Lab. Syst*. **2008**, *92* (1), 83–91. https://doi.org/10.1016/j.chemolab.2007.12.004
54. Andersen, C.M.; Bro, R. Variable selection in regression—a tutorial. *J. Chemometr.* **2010**, *24*, 728- 737. https://doi.org/10.1002/cem.1360
55. Pu, H.; Liu, D.; Wang, L.; Su, D.-W. Soluble solids content and pH prediction and maturity discrimination of lychee fruits using visible and near infrared hyperspectral imaging. *Food Anal. Methods* **2016**, *9*, 235-244. DOI 10.1007/s12161-015-0186-7
56. Gomes., V.M, Fernandes, A.M.; Faia, A.; Melo-Pinto, P. Comparison of different approaches for the prediction of sugar content in new vintages of whole port wine grape berries using hyperspectral imaging, Comput. *Electron. Agric*. **2017**, 140, 244–254. https://doi.org/10.1016/j.compag.2017.06.009
57. Nogales-Bueno, J.; Herna´ndez-Hierro, J.M.; Rodr´iguez-Pulido, F.J.; Heredia, F.J. Determination of technological maturity of grapes and total phenolic compounds of grape skins in red and white cultivars during ripening by near infrared hyperspectral image: a preliminary approach. *Food Chem.* **2014**, *152*, 586–91. https://doi.org/10.1016/j.foodchem.2013.12.030
58. Piazzolla, F.; Amodio, M.L.; Colelli, G.P. Spectra evolution over on-vine holding of Italia table grapes: Prediction of maturity and discrimination for harvest times using a Vis-NIR hyperspectral device. *J. Agric Eng*. **2017**, *48*, 109–116. https://doi.org/10.4081/jae.2017.639
59. Diago, M.P.; Fernández-Novales, J.; Fernandes, A.M.; Melo-Pinto, P.; Tardaguila, J. Use of visible and short-wave near-infrared hyperspectral imaging to fingerprint anthocyanins in intact grape berries. *J. Agric. Food Chem*. **2016**, 64, 7658-7666. https://doi.org/10.1021/acs.jafc.6b01999
60. Chen, S.; Zhang, F.; Ning J.; Liu, X.; Zhang, Z.; Yang, S. Predicting the anthocyanin content of wine grapes by NIR hyperspectral imaging. *Food Chem.* **2015**, 172, 788-793. https://doi.org/10.1016/j.foodchem.2014.09.119
61. Nogales-Bueno, J.; Baca-Bocanegra, B.; Rodriguez-Pulido, F.J.; Heredia, F.J., Hernandez-Hierro, J.M. Use of near infrared hyperspectral tools for the screening of extractable polyphenols in red grape skins. *Food Chem*. **2015**, *172*, 559-564. https://doi.org/10.1016/j.foodchem.2014.09.112
62. Fernandes, A.M.; Oliveira, P.; Moura, J.P.; Oliveira, A.A.; Falco, V.; Correia, M.J.; Melo-Pinto, P. Determination of anthocyanin concentration in whole grape skins using hyperspectral imaging and adaptive boosting neural networks. *J. Food Eng.* **2011**, *105*(2), 216-226. https://doi.org/10.1016/j.jfoodeng.2011.02.018

63. Caporaso, N.; Whitworth, M.B.; Fowler, M.S.; Fisk, I.D. Hyperspectral imaging for non-destructive prediction of fermentation index, polyphenol content and antioxidant activity in single cocoa beans. *Food Chem*. **2018**, 258, 343-351. https://doi.org/10.1016/j.food-chem.2018.03.039
64. Sen, I.; Ozturk, B.; Tokatli, F.; Ozen, B. Combination of visible and mid-infrared spectra for the prediction of chemical parameters of wines. *Talanta* **2016**, *161*, 130–137. https://doi.org/10.1016/j.talanta.2016.08.057
65. Dambergs, R.; Gishen, M.; Cozzolino, D. A review of the state of the art, limitations, and perspectives of infrared spectroscopy for the analysis of wine grapes, must, and grapevine tissue. *Appl. Spectrosc. Rev*. **2015**, *50*, 261-278. https://doi.org/10.1080/05704928.2014.966380